Supporting information for

Microchannel-Confined Crystallization: Shape-controlled Continuous Preparation of High-Quality CL-20/HMX Cocrystal

Li Li[1], Huijun Ling,[1] Jun Tao,[2] Chonghua Pei [1] and Xiaohui Duan*[1]

[1] State Key Laboratory of Environment-friendly Energy Materials Southwest University of Science and Technology, Mianyang 621010, P. R. China
[2] Xi'an Modern Chemistry Research Institute, Xi' an 710065, P. R. China

Email: duanxiaohui@swust.edu.cn

Table S1. Experimental PXRD of CL-20/HMX cocrystal fabricated at solution concentration of 0.25 mol·L^{-1} and flow rate ratio of 1:6.

Table S2. Frequencies of Raman vibrational modes (cm^{-1}) of CL-20/HMX cocrystal fabricated at solution concentration of 0.25 mol·L^{-1} and flow rate ratio of 1:6.

SI 1. Experimental

Caution: CL-20 and HMX are both dangerous high explosives.Unexpected misoperationwas discouraged during this work, Proper safety practices and equipment must be used to prevent explosion due to friction, heat, static shock, or impact. Be aware of the fact that the potential for severe injury exists if these materials are improperly handled.

Materials

Raw CL-20 (the ε polymorph) and raw HMX (the β polymorph), provided by the Institute of Chemical Materials, Chinese Academy of Engineering Physics (CAEP), are white crystalline powders. Dimethyl sulfoxide solution (DMSO, A.R. grade), purchased from Chengdu Ke Long Chemical Reagent Factory, was used as solvent and laboratory-prepared ultra-pure water as anti-solvent.

Cocrystal preparation

First, according to the molar ratio 2:1 of CL-20 and HMX in CL-20/HMX cocrystal, three transparent DMSO solutions of CL-20 and HMX were prepared through ultrasonic stirring. The corresponding concentrations were 0.083, 0.125 and 0.25 mol·L-1, respectively. Here, the concentration value was denoted only as the concentration of CL-20 in solution. Then, the solution was fed into the left horizontal channel of the flow-focusing microreactor at the fixed flow rate of 1 mL/min; the anti-solvent was fed into the upper and lower vertical channels applying variable flow rates. Flow rate was controlled by the peristaltic pump(BT100-1L) with flow range of 0.002-500 mL/min and accuracy of 0.001 mL/min. The solution and anti-solvent efficiently mixed at the intersection of the flow-focusing microchannel and immediately seed out due to high instantaneous supersaturation. The resulting slurry flowed through the right horizontal channel in 9 cm length and entered into the collector. Namely, the residence time was also fixed, and the tuneable parameters are only solution concentration and flow rate ratio of solution and anti-solvent. The whole process was carried out at room temperature (25°C). Subsequently, the slurry in collector was filtered and then washed 3-5 times using ultra-pure water to remove the solvent. Finally, the sample was put into the vacuum freeze-drying machine for 5 h pre-freezing and 36 h freeze drying at -65°C to give a white powder. The total recovery was about 97±1%.

Characterization

SEM was conducted on an ULTRA 55 (ZEISS, Germany) field emission scanning electron microscope, which was operated at 7 kV acceleration voltage and equipped with energy dispersive X-ray spectroscopy (EDS).

XRD data were recorded by a PANalyticalX'pert PRO X-ray diffractometer (40 kV, 40 mA) equipped with a copper anode (Cu Kα radiation, λ = 1.54187 Å). The measurement was performed using a 2θ scan range from 3 to 80°. Simulated XRD patterns were generated from the single-crystal structure of CL-20/HMX cocrystal reported by Matzger et al. (CCDC 875458) using Reflex module in Materials Studio 3.0. The simulation paraters were set mainly according to the experimental condition, and other parameters adopted the default setting of Reflex module.

The density measurement was carried out on a micromeriticsAccuPyc II 1340 V2.00 taking He as analysis gas. The average chamber temperature was close to 300 K and equilibration pressure change was set to the standard 0.345 hPa. A calibration for the chamber volume was carried out before the measurement. The sample mass was about 10 g weighed using the Sartorius BSA124S analytical balance with an accuracy of 0.1 mg. Three hundred flushing cycles ensured the total sample dryness during the measurement. Three true repeat measurements were performed and between 50 and 300 data points were collected for each measurement.

Particle size was determined using a Malvern Mastersizer v3.5 with dispersion medium of 2-propanol and agitation speed of 2450 rpm. A refractive index of 1.69 was chosen, and the absorption coefficient was selected individually for the best results. The result was an average of three measurements, each consisting of 10 000 individual scans.

The crystal quality was further analyzed by optical polarizing microscope (OPM) with matching refractive index. The crystals were immersed in a mixture of 1-methyl naphthalene and decan (8:1) to highlight the intermal defects of the crystals.

Performance tests

The thermal decomposition properties were determined by differential scanning calorimetry/thermogravimetry (DSC/TG) using a Jupiter STA449C synchronous thermal analyzer in a N2 atmosphere with heating rate of 10°C/min. The decomposition reaction was investigated by TG-FTIR, which was documented by the Jupiter STA449C simultaneous thermal analyzer coupled with FTIR (TENSOR Ⅱ). CL-20/HMX sample of ≈0.6 mg in aluminum crucibles (80 μL) was heated at a heating rate of 10 °C min^{-1} in N_2 atmosphere.

According to GJB5891.22-2006 method, the impact sensitivity expressed as impact energy was tested by a BAM Fall hammer device (BFH-PEx, America) with 2 kg drop weight. The limiting impact energy was obtained as the explosion occurs in at least one trial in six. Each sample (30±1 mg) was tested 30 times. According to GJB 5891.24-2006 method, the friction sensitivity was performed by a friction sensitivity instrument (FSKM 10L, America). Each sample (20±1 mg) was tested 30 times. In these cases, the atmospheric temperature was 25 °C and the humidity was 85% RH.

SI 2. SEM images of CL-20/HMX cocrystal fabricated with different flow rate ratios under the concentration of 0.083 mol·L^{-1}.

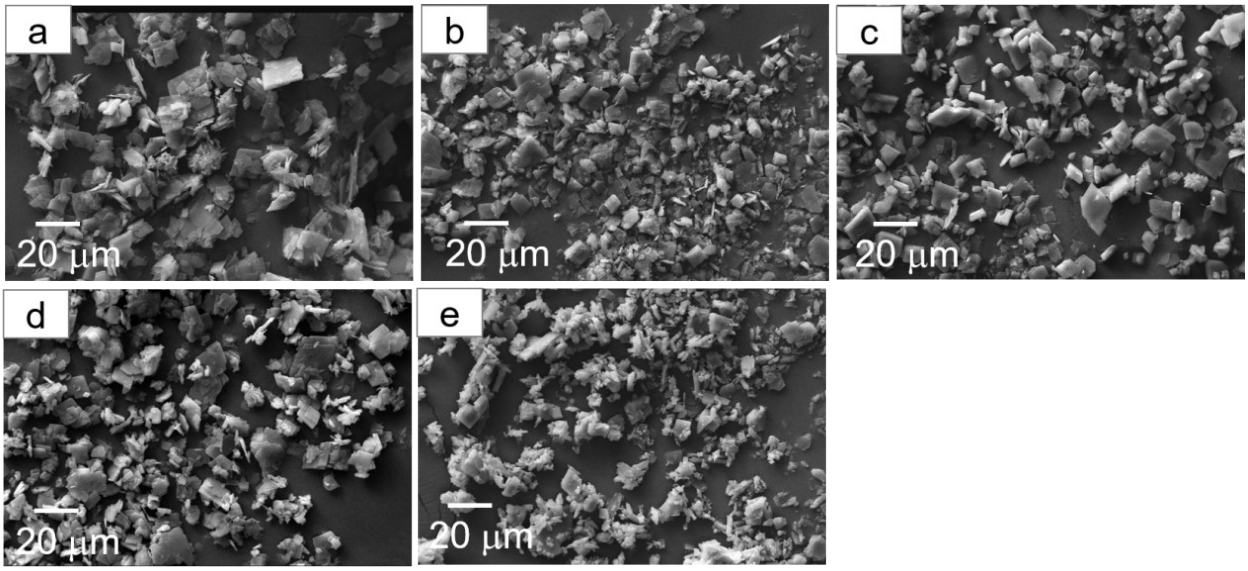

Fig. S1. SEM images of samples with different flow rate ratios of 1:2 (a), 1:4 (b), 1:8 (c), 1:16 (d) and 1:32 (e) under the concentration of 0.083 mol·L^{-1}.

SI 3. PXRD patterns of CL-20/HMX cocrystal fabricated with different flow rate ratios under the concentration of 0.083 mol·L^{-1}.

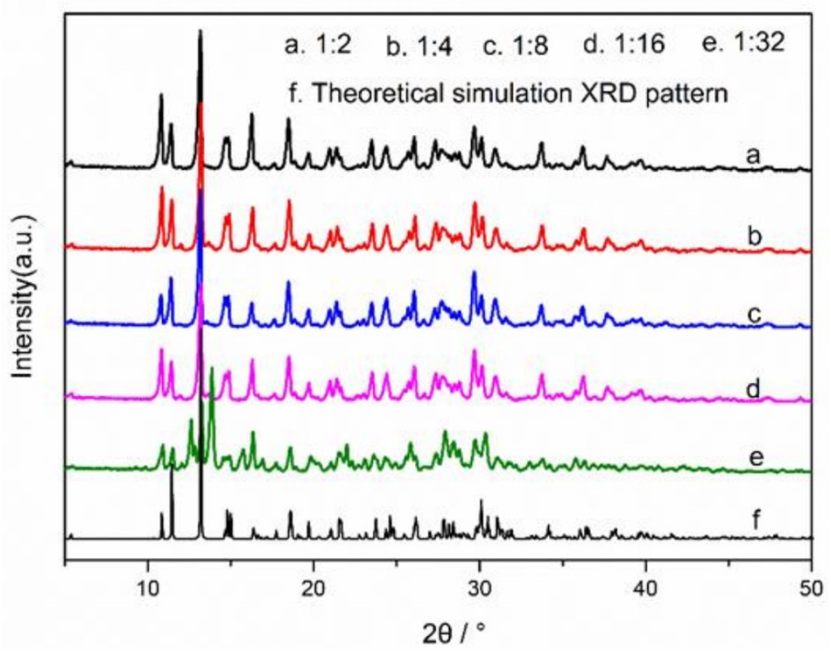

Fig. S2 PXRD patterns of samples with different flow rate ratios under the concentration of 0.083 mol·L^{-1}.

SI 4. DSC-TG curves of CL-20/HMX cocrystal fabricated with different flow rate ratios under the concentration of 0.083 mol·L^{-1}.

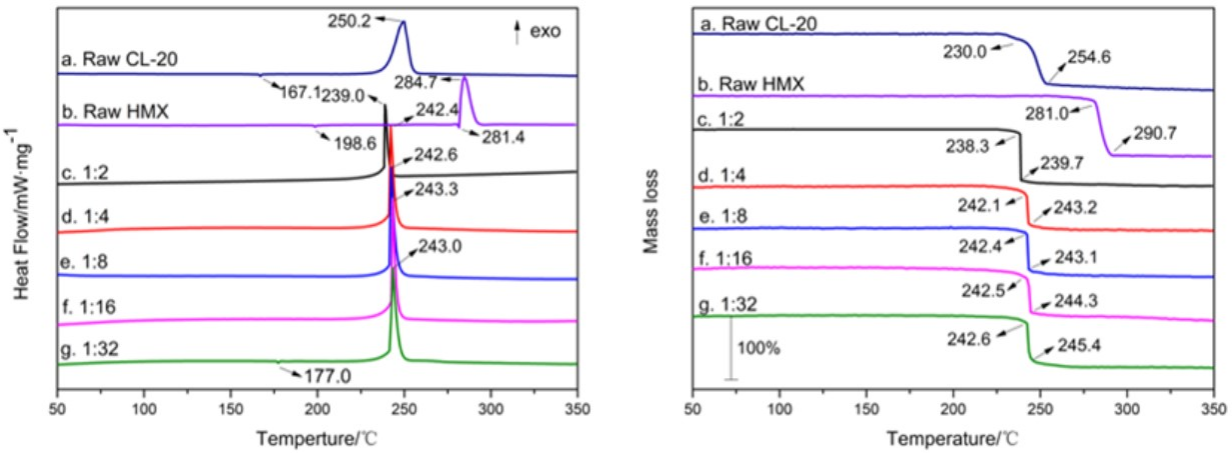

Fig. S3 DSC-TG curves of samples with different flow rate ratios under solution concentration of 0.083 mol·L^{-1}.

SI 5. SEM images of CL-20/HMX cocrystal fabricated with different flow rate ratios under the concentration of 0.125 mol·L^{-1}.

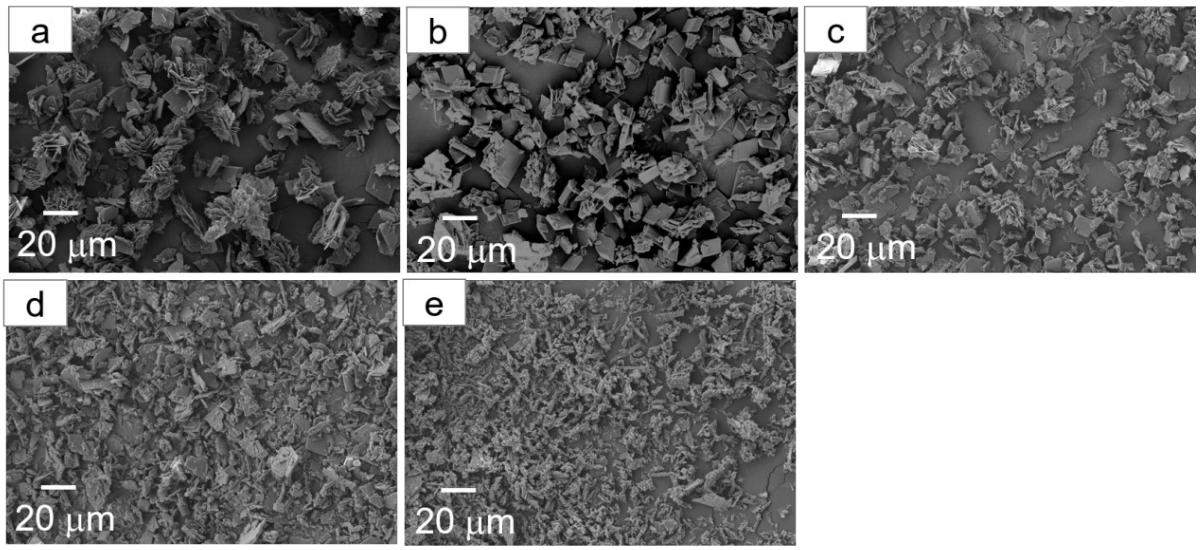

Fig. S4. SEM images of samples with different flow rate ratios of 1:2 (a), 1:4 (b), 1:8 (c), 1:16 (d) and 1:32 (e) under the concentration of 0.125 mol·L^{-1}.

SI 6. PXRD patterns of CL-20/HMX cocrystal fabricated with different flow rate ratios under the concentration of 0.125 mol·L^{-1}.

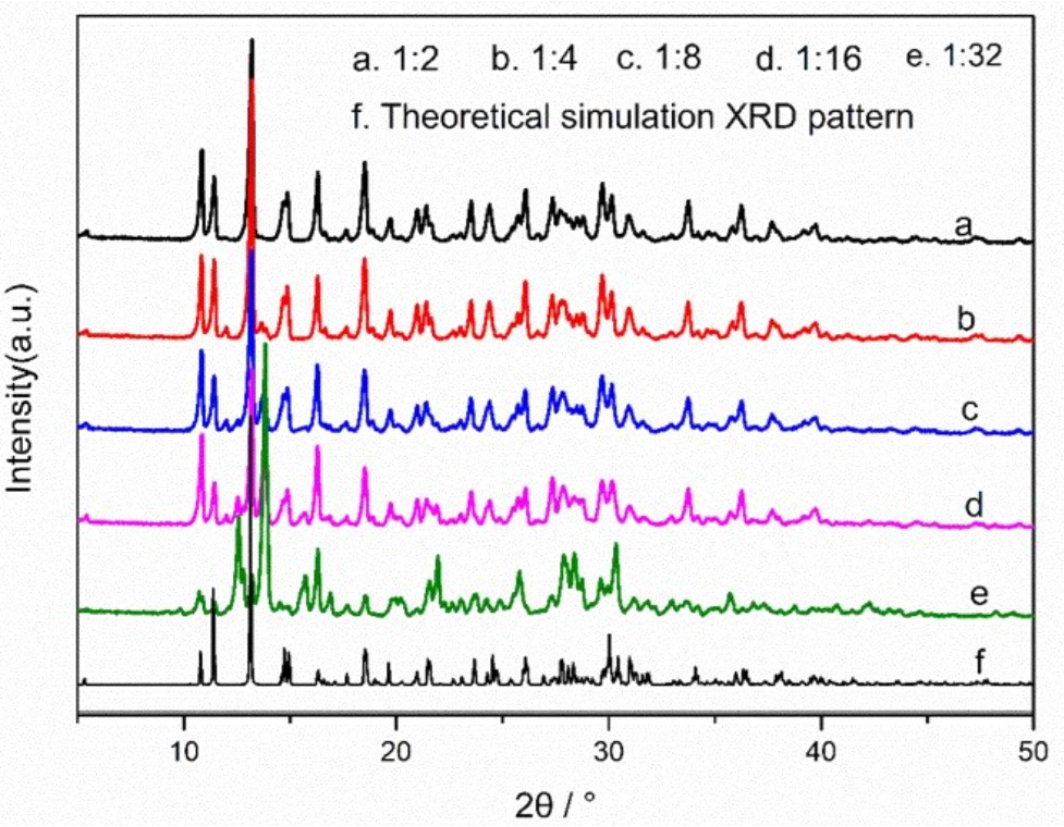

Fig. S5 PXRD patterns of samples with different flow rate ratios under the concentration of 0.125 mol·L^{-1}.

SI 7. DSC-TG curves of CL-20/HMX cocrystal fabricated with different flow rate ratios under the concentration of 0.125 mol·L^{-1}.

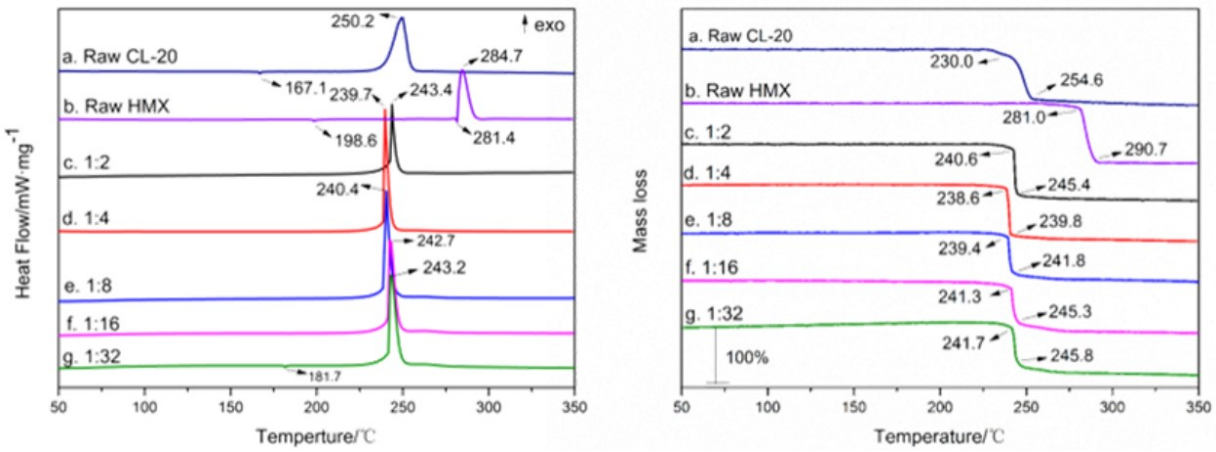

Fig. S6 DSC-TG curves of samples with different flow rate ratios under solution concentration of 0.125 mol·L^{-1}.

SI 8. SEM images of CL-20/HMX cocrystal fabricated with different flow rate ratios under the concentration of 0.25 mol·L^{-1}.

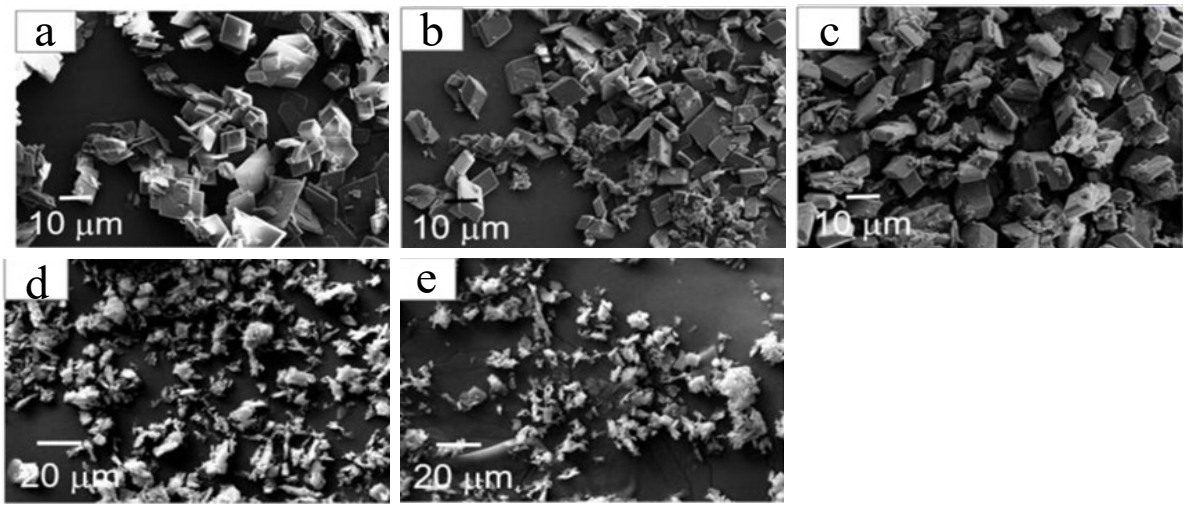

Fig. S7. SEM images of samples with different flow rate ratios of 1:2 (a), 1:4 (b), 1:8 (c), 1:16 (d) and 1:32 (e) under the concentration of 0.25 mol·L^{-1}.

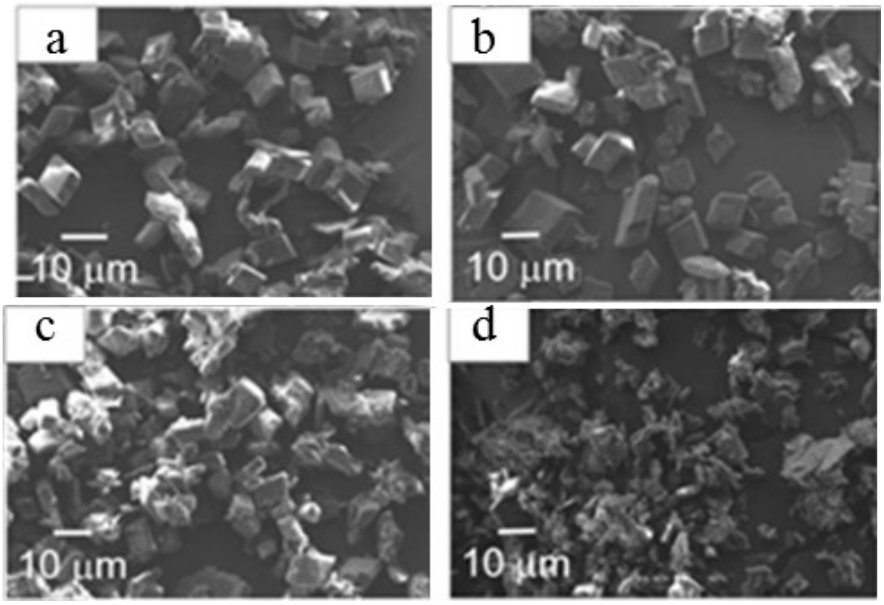

Fig. S8. SEM images of samples with different flow rate ratios of 1:6 (a), 1:10 (b), 1:12 (c) and 1:14 (d) under the concentration of 0.25 mol·L^{-1}.

SI 9. PXRD patterns of CL-20/HMX cocrystal fabricated with different flow rate ratios under the concentration of 0.25 mol·L^{-1}.

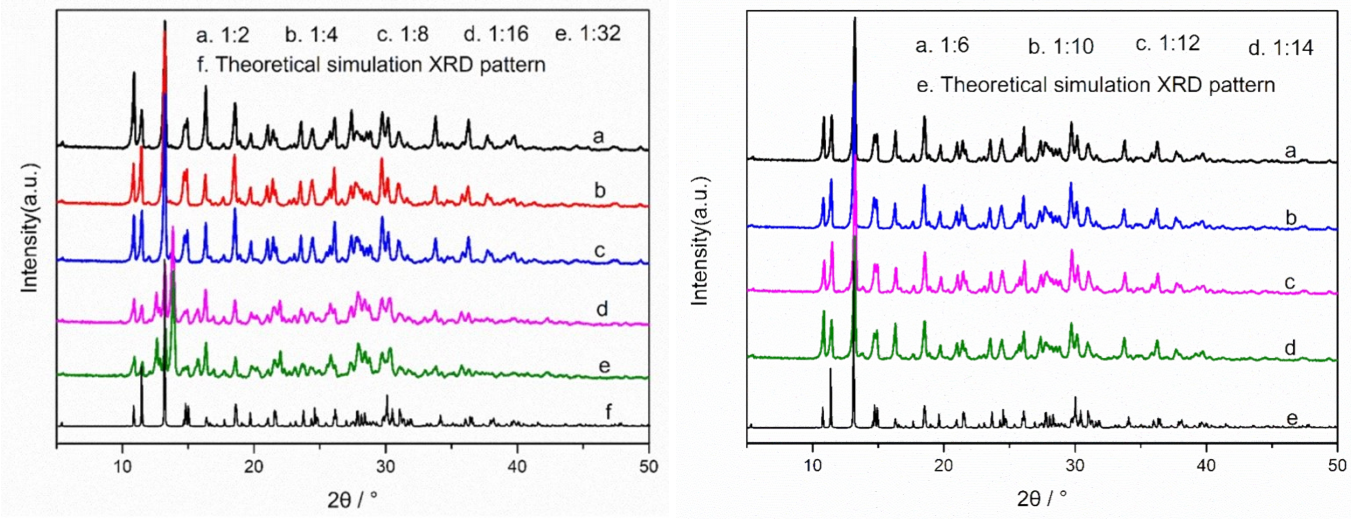

Fig. S9 PXRD patterns of samples with different flow rate ratios under the concentration of 0.25 mol·L^{-1}.

SI 10. DSC-TG curves of CL-20/HMX cocrystal fabricated with different flow rate ratios under the concentration of 0.25 mol·L^{-1}.

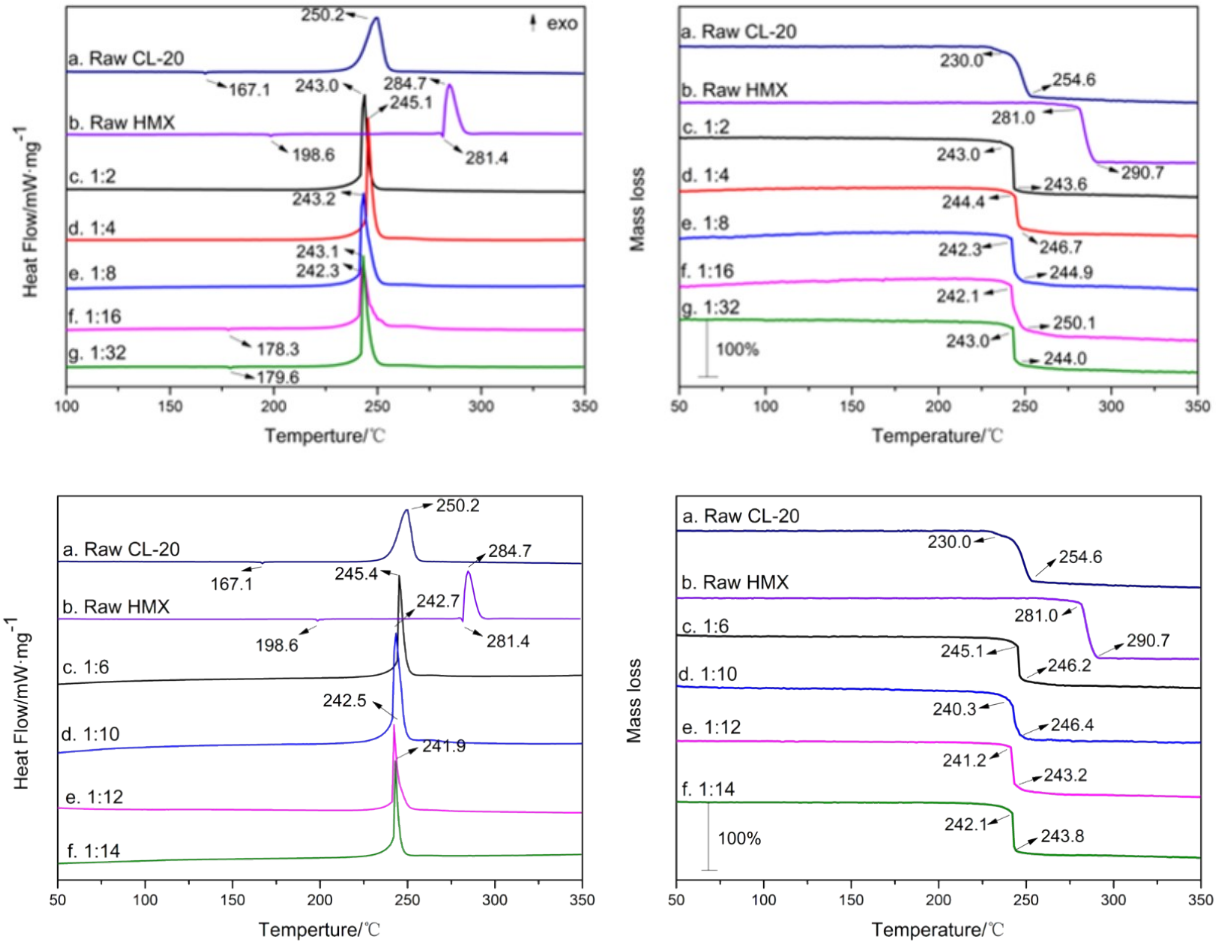

Fig. S10 DSC-TG curves of samples with different flow rate ratios under solution concentration of 0.25 mol·L^{-1}.

SI 11. OPM images of CL-20/HMX cocrystal fabricated at solution concentration of 0.25 mol·L^{-1} and flow rate ratio of 1:6.

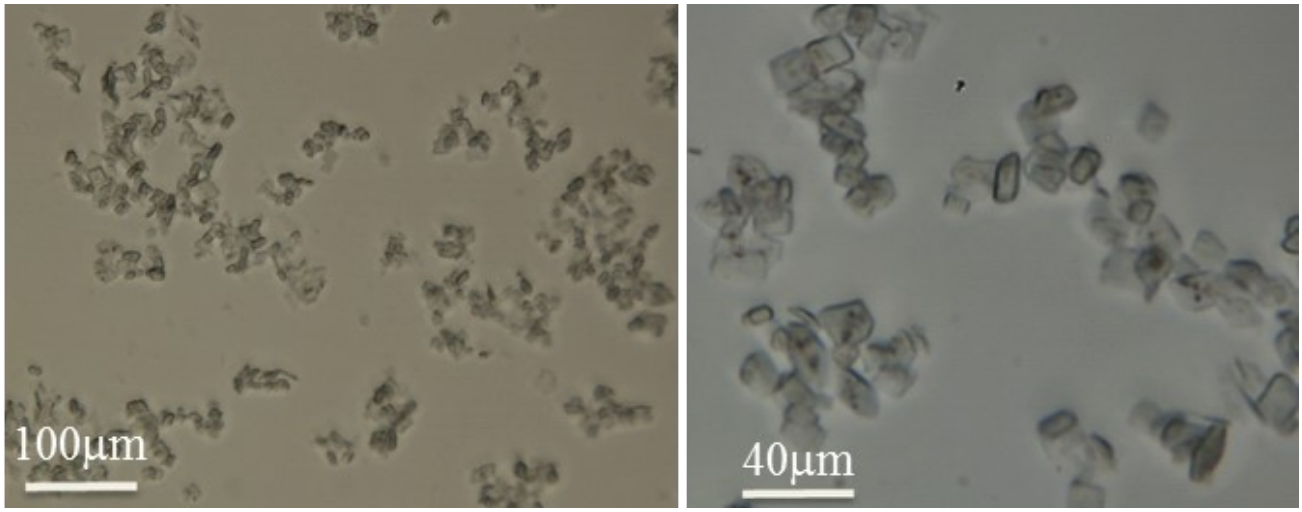

Fig. S11. OPM images of CL-20/HMX cocrystal fabricated at solution concentration of 0.25 mol·L^{-1} and flow rate ratio of 1:6.

SI 12. Raman spectra of CL-20/HMXcocrystal fabricated at solution concentration of 0.25 mol·L^{-1} and flow rate ratio of 1:6.

Spectra were collected in extended scan mode in the range of 3000-100 cm^{-1} and then analyzed using the Labspec 5.0 software package. Calibration was performed using a silicon standard.

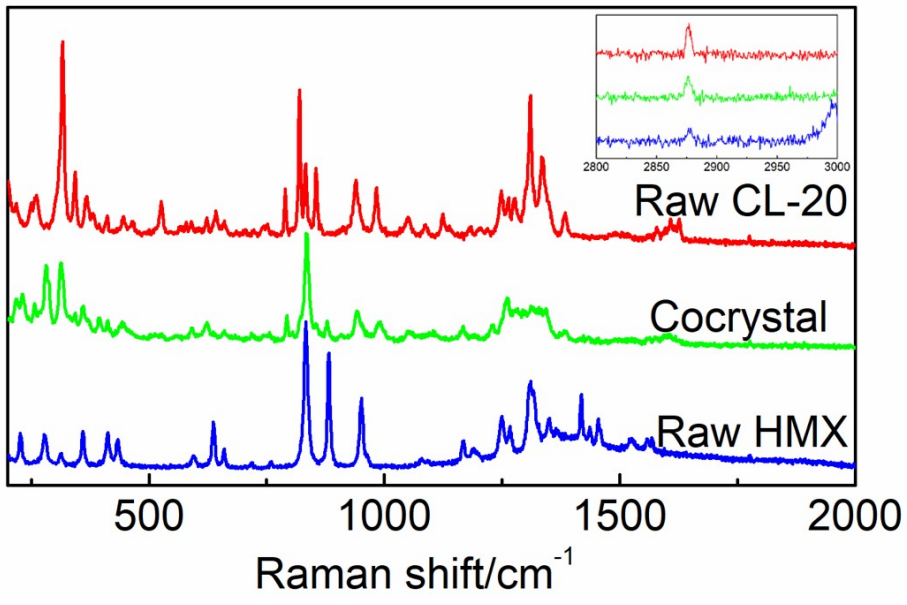

Fig. S12. Raman vibrational modes (cm^{-1}) of CL-20/HMX cocrystal fabricated at solution concentration of 0.25 mol·L^{-1} and flow rate ratio of 1:6.

SI 13. FT-IR (cm^{-1}) of CL-20/HMX cocrystal fabricated at solution concentration of 0.25 $mol \cdot L^{-1}$ and flow rate ratio of 1:6.

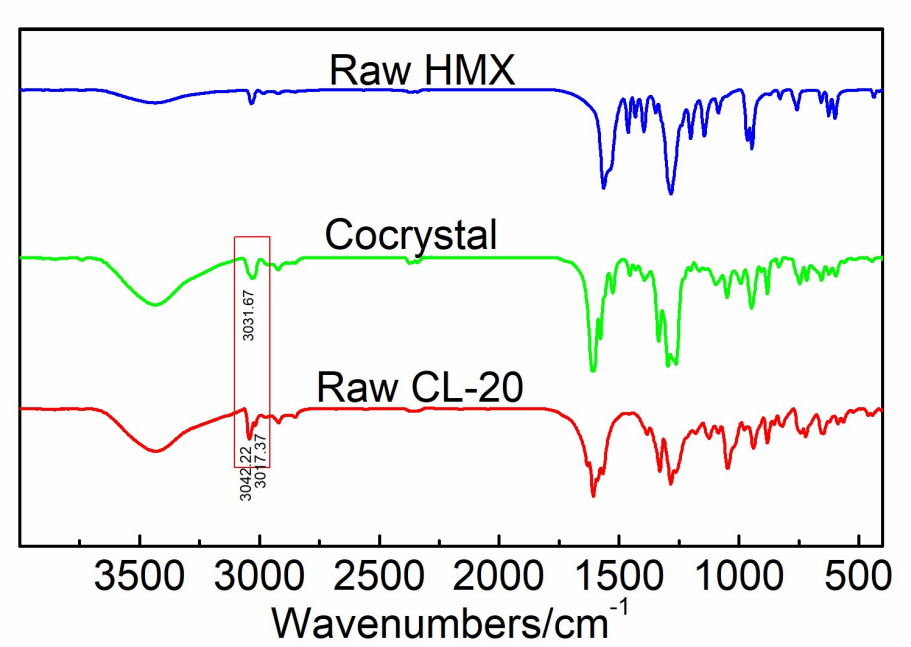

Fig. S13. FT-IR (cm^{-1}) of CL-20/HMX cocrystal fabricated at solution concentration of 0.25 $mol \cdot L^{-1}$ and flow rate ratio of 1:6.

SI 14. TG curves of CL-20/HMX co-crystal fabricated at solution concentration of 0.25 $mol \cdot L^{-1}$ and flow rate ratio of 1:6.

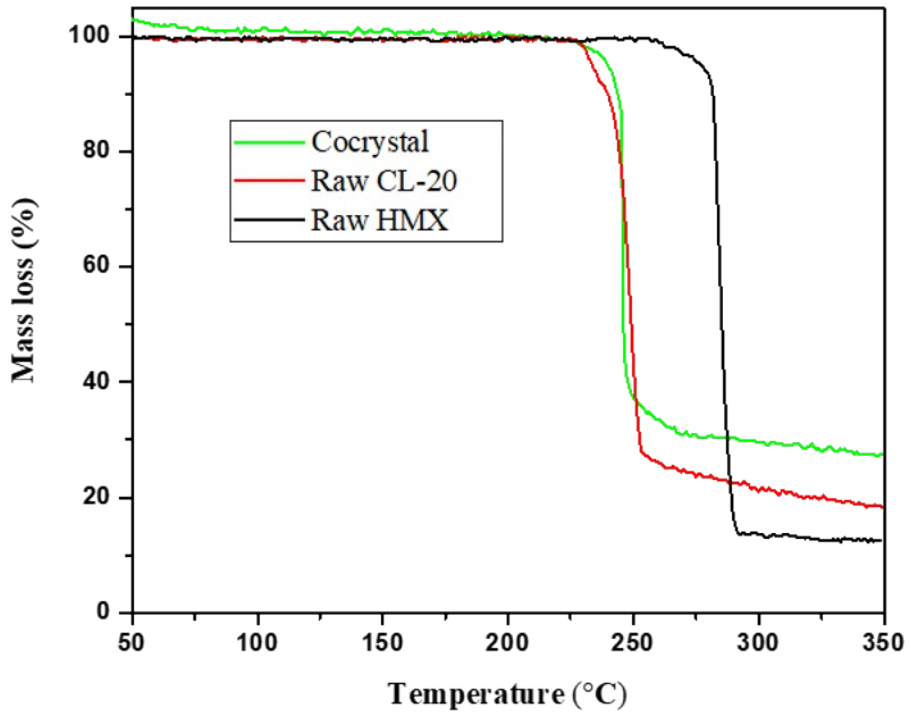

Fig. S14. TG of CL-20/HMX cocrystal obtained at solution concentration of 0.25 $mol \cdot L^{-1}$ and flow rate ratio of 1:6.

Table S1. Experimental PXRD of CL-20/HMX cocrystal fabricated at solution concentration of 0.25 mol·L^{-1} and flow rate ratio of 1:6.

2θ(°)	FWHM (°)	I/I_0(%)		2θ(°)	FWHM (°)	I/I_0(%)
5.411	0.177	3		34.202	0.178	2.9
10.852	0.203	44.4		34.666	0.279	2.9
11.431	0.187	30.6		34.993	0.143	2.5
13.199	0.2	100		35.826	0.282	6.1
14.875	0.311	23.7		36.236	0.242	16.8
16.308	0.211	34.1		36.976	0.135	1.4
17.127	0.056	0.7		37.672	0.304	8.6
17.65	0.165	4.7		39.173	0.407	4.2
18.517	0.223	38.6		39.739	0.424	7.8
18.857	0.436	4.9		40.277	0.149	1.5
19.72	0.235	10.3		40.895	0.269	1.1
20.231	0.239	1.7		41.214	0.375	2.2
20.991	0.269	15.3		42.293	0.111	0.9
21.421	0.32	17.3		42.795	0.521	1.7
23.028	0.294	3.2		43.384	0.362	1.7
23.527	0.188	18.8		44.483	0.318	2.1
24.399	0.246	17.2		44.822	1.064	1.2
25.736	0.472	11.5		45.385	0.15	1.2
26.096	0.227	24.2		47.233	0.435	2.7
26.691	0.119	1.9		49.305	0.192	1.8
27.37	0.278	19.8		50.435	0.199	0.7
27.713	0.778	13.6		51.935	0.533	0.8
27.972	0.976	10.1		52.48	0.669	1.3
28.784	0.255	10.4		53.05	0.242	2.2
29.711	0.279	27		55.749	0.247	1.3
30.145	0.276	20.5		57.252	0.405	1.1
30.951	0.296	11		59.282	0.484	1.4
31.62	0.154	2.7		59.654	0.127	0.9
32.958	0.211	2		60.877	0.268	0.7
33.754	0.235	18.6		62.707	0.23	0.7

Table S2. Frequencies of Raman vibrational modes (cm^{-1}) of CL-20/HMX cocrystal fabricated at solution concentration of 0.25 $mol \cdot L^{-1}$ and flow rate ratio of 1:6.

220.154	659.666	1262.74
232.368	721.05	1293
256.718	756.545	1310.34
280.966	792.817	1328.53
312.775	833.836	1387.21
343.321	878.503	1608.5
360.703	945.311	2876.38
394.232	991.975	2960.79
412.536	1050.7	
446.831	1106.88	
591.35	1167.16	
623.542	1232.31	